Exploring the effects of bay position chlorination on the emissive properties of chloro-(chloro)$_n$-boron subnaphthalocyanines for light emission.

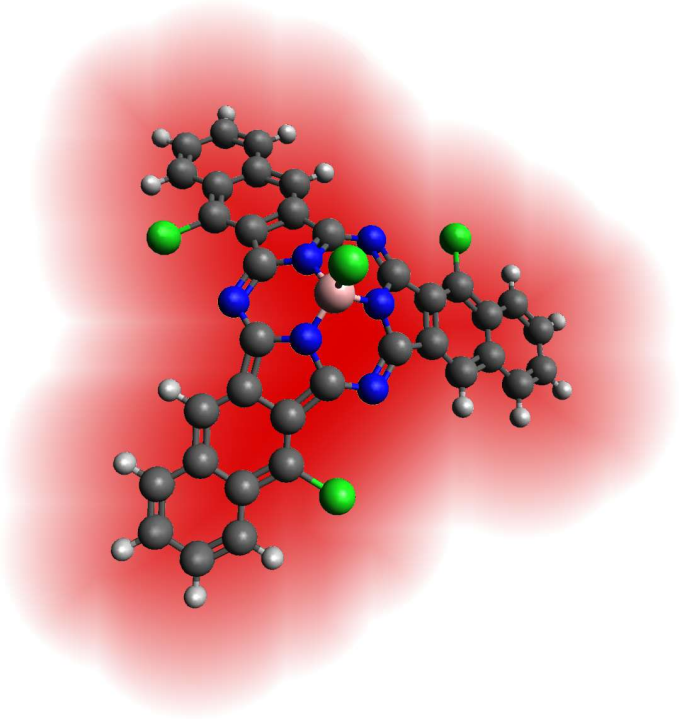

Saul T. E. Jones [a], *Andrew J. Pearson* [a], *Jeremy D. Dang* [b], *Neil C. Greenham* [a], *Timothy P. Bender* [*,b,c,d], *and Dan Credgington* [*,a]

[a.] Cavendish Laboratory, J.J. Thomson Avenue, Cambridge CB3 0HE, United Kingdom.

[b.] Department of Chemical Engineering and Applied Chemistry, University of Toronto, 200 College St., Toronto, Ontario, Canada M5S 3E5.

[c.] Department of Chemistry, University of Toronto, 80 St. George St., Toronto, Ontario M5S 3H6, Canada.

[d.] Department of Materials Science and Engineering, University of Toronto, 184 College St., Toronto, Ontario, Canada M5S 3E4.

Corresponding Authors

* - to whom correspondences should be addressed. Email: tim.bender@utoronto; dan.credgington@gmail.com.

ABSTRACT

It has been previously found that through an established synthesis of the macrocycle boron subnaphthalocyanine (BsubNc) that random bay-position chlorination occurs and results in a mixed alloyed composition that cannot be separated; called chloro-(chloro$_n$)-boron subnaphthalocyanines (Cl-Cl$_n$BsubNcs). Through modifications of the synthetic method, amounts of the average bay-position chlorination can be varied. Cl-Cl$_n$BsubNcs are fluorescent and therefore here we explore the effect of the amount of bay-position chlorination on the photoluminescent and electroluminescent properties of Cl-Cl$_n$BsubNcs. Distinct from previous reports detailing the positive impact of higher average bay-position chlorination, we find that the photophysical processes important to OLEDs improve with lower average bay-position chlorination. A higher degree of bay-position chlorine shows higher nonradiative recombination rates, lower photoluminescence quantum efficiencies and a basic OLEDs exhibits a greater host emission fraction, implying less effective energy transfer. These results advance the consideration of subnaphthalocyanines for light-emitting and optoelectronic applications.

Introduction.

Boron subnaphthalocyanines (BsubNcs, Figure 1) are a subgroup of the phthalocyanine macrocyclic family, which have attracted interest as functional organic semiconductors[1–4] and sensor materials[5] because of their synthetic tunability[6–9] and high thermal, chemical and photo-stability.[10–12] Structurally BsubNcs, and their counterparts boron subphthalocyanine (BsubPc),[13] differ from conventional metal- and metalloid-phthalocyanines (MPcs)[14] because of their molecular non-planar conformation and reduced trimeric ligand structure. The extended π-conjugation of BsubNc relative to BsubPc results in a narrowing of the semiconductor bandgap, with peak absorption and luminescence shifted towards the red / near-IR regions of the light spectrum. As is typical of MPcs, additional functionalization may be achieved via coordination of substituent atoms and molecules to the axial and/or bay positions, opening up a vast array of materials for applications as diverse as dyes, pigments, organic field-effect transistors (OFETs), organic light-emitting diodes (OLEDs), organic photovoltaics (OPVs) and photodynamic therapy. [10,15]

Within the OPV research space Cl-BsubPc has arguably acted as the archetypal BsubPc material, with its *n*-type character identifying it as a potential non-fullerene electron acceptor.[1,16–20] BsubPcs have also shown promise as electron donor materials[21] and triplet harvesters.[22] BsubPcs have been incorporated into planar heterojunction OPVs[1,23–28] as well as bulk-heterojunction OPVs as solution cast materials,[29,30] demonstrating the versatile nature of these molecules.

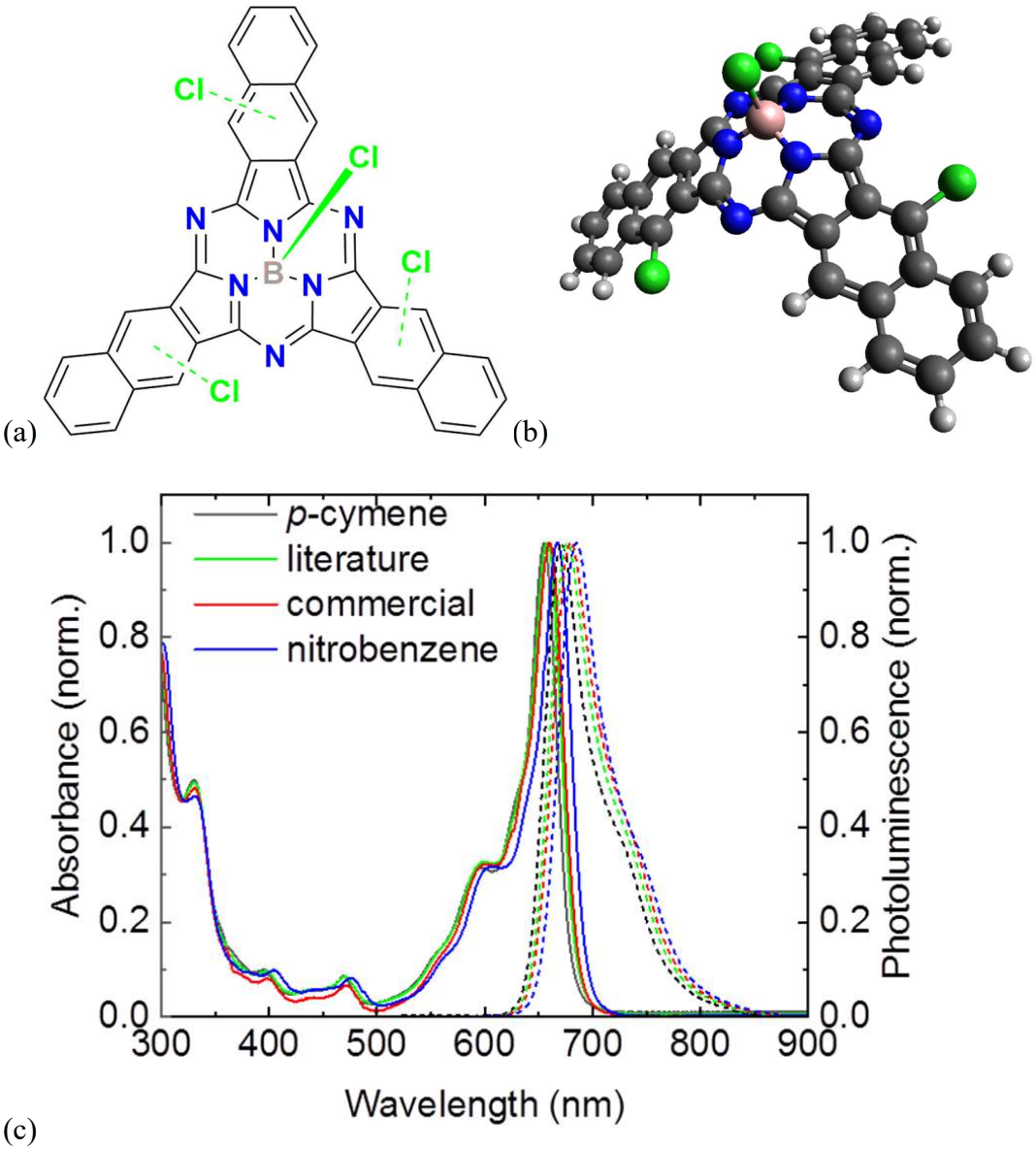

Figure 1. (a) The 2D and **(b)** 3D chemical structure of chloro-(chloro$_n$)-boron subnaphthalocyanines (Cl-Cl$_n$BsubNcs) highlighting the random bay-positions that can be functionalized with Cl through the synthetic process, and **(c)** UV-vis and photoluminescence spectra for the different batches of Cl-Cl$_n$BsubNc used in this study. For PL measurements, an excitation wavelength of 407 nm was used. The solid lines show the absorption and the dashed lines show the photoluminescence. Further details of the set of chemical structures enabling the mixed alloyed composition are presented in Figure S1.

Dang *et al*. illustrated that the chemical process reported to produce Cl-BsubNc yields a mixed alloyed composition of BsubNc with random bay-position chlorination.[2] Variations in chemical processes were demonstrated to reproducibly vary the amount of bay-position chlorination and we hereafter refer to these materials as Cl-Cl_nBsubNc(s) where n is the degree of random bay position chlorination. OPVs utilising Cl-Cl_nBsubNcs with higher chlorine content were found to perform the best within an OPV due to a relatively large fill factor (53%) which was sufficient to offset a small reduction in open-circuit voltage (V_{oc}) compared to OPVs utilizing Cl-Cl_nBsubNcs with lower chlorination levels.[2] A similar trend was shown when Cl-Cl_nBsubNcs where applied as electron donating materials.[4] It has also been shown that mixed alloyed composition remains constant on further chemical derivatization of Cl-Cl_nBsubNc and enables their integration into bulk-heterojunction OPVs.[9]

In contrast with the developments in OPVs, far fewer reports exist on the applications of BsubPcs and BsubNcs as emissive materials in OLEDs. This fact may seem surprising given the relatively high luminescence quantum efficiencies and narrow emission bandwidths that can be achieved in dilute systems. In 2007 Díaz *et al.* published the first report on a series of BsubPc derivatives exhibiting narrow luminescence spectra (full-width at half-maximum values ranging from 60 to 90 nm) centred between 580 and 620 nm.[31] For BsubPcs with 4-*tert*-butylphenoxy as the axial group, photoluminescence quantum efficiencies (PLQEs) of up to 56% in solution were measured. Integration of the BsubPcs into an OLED, where the active layer comprised BsubPcs diluted within a Spiroblue matrix, resulted in devices exhibiting narrow electroluminescence (EL) in the red-orange region with negligible residual emission from the host.[31] Vacuum-processed OLEDs with fluorinated phenoxy BsubPc as the emissive layer exhibit pure orange EL[32,33] and Cl-BsubPc and Cl-BsubNcs exhibit "warm white" EL[34]. Although the performance metrics of these

OLEDs were low (0.03 to 1.5 cd A^{-1}), this work demonstrated the potential for BsubPcs as active layer materials in light-emitting applications, particularly where high spectral purity is sought. The first example of BsubNcs as emitting materials within OLEDs has also been demonstrated, showing a mixture of host (Alq3) and guest emission, with a peak EQE 0.41% .[34]

Given the potential of Cl-Cl_nBsubNc as light emitting materials, we wish to understand the influence on the degree of bay-position chlorination on their luminescence properties. Here we report on the luminescence properties of Cl-Cl_nBsubNcs with varying amounts of bay-position chlorination, and demonstrate that photoluminescence yield improves and non-radiative rate decreases with lower average bay-position chlorination. We show that when Cl-Cl_nBsubNc is diluted within a poly(9,9-dioctylfluorene-co-benzothiadiazole) (F8BT) host, OLED devices displaying narrow electroluminescence (EL) around 680 nm and external quantum efficiencies (EQEs) of up to 0.9 % at 100 cd m^{-2} (current efficiency of 2.5 cd A^{-1}) can be achieved. We show that electroluminescence of Cl-Cl_nBsubNcs follows the same trend as photoluminescence, with lower average bay-position chlorination leading to better OLED device performance. In particular, Cl-Cl_nBsubNcs with higher average chlorination exhibit less effective energy transfer from the host at equivalent doping concentration, resulting in greater host emission at high current densities. These findings are important for the development of MPcs, BsubNcs and BsubPcs in general, as they demonstrate that even for synthetic pathways where mixed-alloyed samples are produced, trends that impart favourable structural and/or optoelectronic properties can still guide the direction of future synthesis strategies.

Results and Discussion.

The synthetic routes for producing Cl-Cl$_n$BsubNc with varying average bay-position chlorination have previously been reported;[2] here is the identical nomenclature that was used and published to distinguish the different samples: literature-Cl-Cl$_n$BsubNc (synthesized by the literature procedure), *p*-cymene-Cl-Cl$_n$BsubNc (utilizing *p*-cymene in the reaction to limit bay-position chlorination) and nitrobenzene-Cl-Cl$_n$BsubNc (utilizing nitrobenzene in the reaction to maximize bay-position chlorination). The three variants can be differentiated as follows: the literature route follows the method reported by Zyskowski and Kennedy[23] where 2,3-dicyanonaphthalene is reacted with BCl_3 in dry 1,2-dichlorobenzene at 180 ˚C; the *p*-cymene route substitutes 1,2-dichlorobenzene for a mixture of 1,2,4-trichlorobenzene: *p*-cymene (4:1 vol%), with the cymene solvent acting as a chlorine scavenger to enable limited bay-position chlorination; the nitrobenzene route involves the use of nitrobenzene fully as the reaction solvent, which due to its limited chlorine scavenging properties affords the synthesis of Cl-Cl$_n$BsubNc with high bay-position chlorination. Thus, the three routes lead to the production of Cl-Cl$_n$BsubNc with intermediate, low and high chlorine content respectively. XPS analysis determined the average bay-position chlorination to be 1.21, 0.18 and 4.17 atoms per molecule respectively (literature, *p*-cymene, nitrobenzene).[2] A batch of Cl-Cl$_n$BsubNc sourced from a commercial supplier (commercial) is also investigated here; bay-position chlorination was determined by XPS to be 1.61.[2] Each synthetic procedure produces mixtures of Cl-Cl$_n$BsubNc with different molecules containing anywhere between 0 and 6 Cl atoms at random bay positions (Figure S1). No synthesis route is currently developed to set the degree of bay-chlorinated Cl-Cl$_n$BsubNc precisely at 0 or 6, however the average degree of chlorination in the batches considered here provides a parameter against which photophysical and device trends can be correlated.

Table 1.

Optoelectronic properties of Cl-Cl_nBsubNc prepared by each synthesis route where (*n*) is the average degree of bay-position chlorination as measured by XPS[2], (E_g) is the optical band gap, ($\lambda_{Max, Abs}$) and ($\lambda_{Max, PL}$) are the absorption and PL peak wavelengths respectively, (PLQE) is the Photo Luminescence Quantum Efficiency, (*k*) is the PL decay lifetime, (k_r) is the radiative rate, (k_{nr}) is the non-radiative rate, (HOMO) measured with UPS, (LUMO) estimated as the HOMO energy+E_g. All optical measurements carried out on dilute solutions in chlorobenzene. Steady state PL spectra and PLQE were excited at 600nm with a monochromated xenon lamp. Transient PL measurements were excited using a pulsed 375nm laser.

	n	E_g / eV	$\lambda_{Max, Abs}$ [b] / nm	$\lambda_{Max, PL}$ [c] / nm	PLQE [d] / %	k [e] / 10^8 s^{-1}	k_r / 10^8 s^{-1}	k_{nr} / 10^8 s^{-1}	HOMO [f] / eV	LUMO [g] / eV
***p*-cymene -Cl-Cl_nBsubNc**	0.18	1.82	655	675	28	2.94	0.85	2.09	5.29	3.47
literature -Cl-Cl_nBsubNc	1.21	1.81	657	680	27	3.03	0.82	2.21	5.31	3.5
commercial -Cl-Cl_nBsubNc	1.61	1.81	660	684	24	3.22	0.77	2.45	5.31	3.5
nitrobenzene -Cl-Cl_nBsubNc	4.17	1.79	667	689	22	3.44	0.72	2.72	5.42	3.63

The photoluminescence properties of each Cl-Cl_nBsubNc mixture were characterized in dilute solution, pure film and host:guest film. As presented in Figure 1 and Table 1, each mixture exhibits a relatively sharp Q-band absorption feature around 660 nm,[24] with photoluminescence most intense around 680 nm. Increasing the level of bay-position chlorination results in a reduction in Cl-Cl_nBsubNc optical bandgap and red-shifted emission. We confirmed that the PL and absorption

spectra of these materials series in the solid neat thin films are consistent with those reported previously (Figure S2). In dilute solution the emission profile for each mixture remains relatively narrow, with full-width at half-maximum (FWHM) values ranging between 52 and 58 nm [140 to 150 meV] (Table S1). PLQEs were determined using an absolute method for dilute Cl-Cl$_n$BsubNc solutions in chlorobenzene (Table 1), and show that lower bay position chlorine content is correlated with higher PLQE.[2]

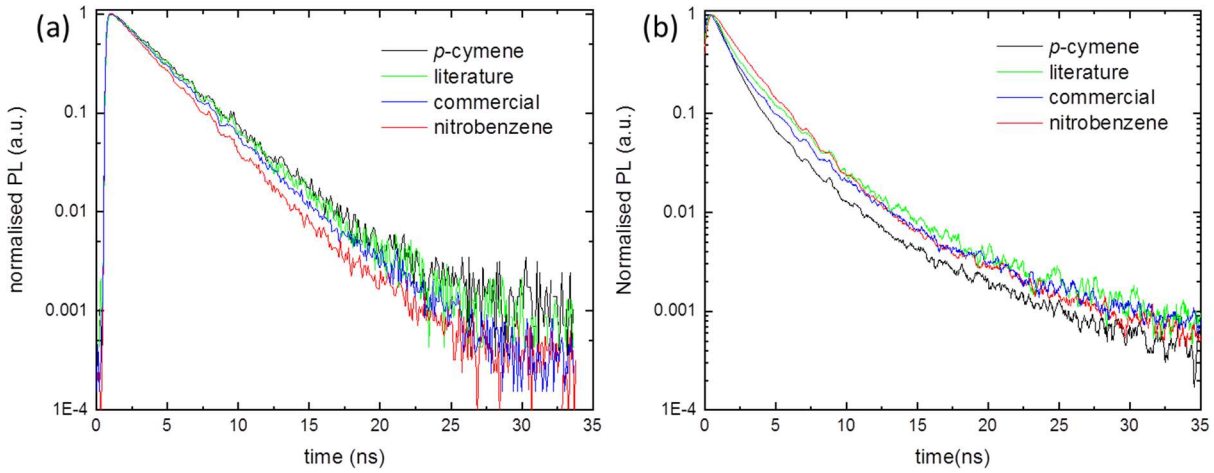

Figure 2. PL decay kinetics of Cl-Cl$_n$BsubNc dilute solutions (0.02 mg ml^{-1} in CB) (a) and Cl-Cl$_n$BsubNc:F8BT (1:99 wt%) host:guest thin films that are representative of the OLED active layers (b).

All compounds exhibit single-component exponential photoluminescence decay kinetics with lifetimes ranging from 2.9 ns (nitrobenzene) to 3.4 ns (*p*-cymene) (Figure 2). We therefore conclude that singlet fluorescence is dominant in these systems. The lower PLQE of nitrobenzene-Cl-Cl$_n$BsubNc arises from a higher nonradiative decay rate (Table 1). Both the changes observed in PLQE and more rapid fluorescence lifetimes would be consistent with more rapid intersystem

crossing due to heavy atom effects from the Cl atoms, as has been observed in dichloroanilines and bromine-functionalised bianthryl. [25,35–37]

To establish if these trends extend to electroluminescence in devices, each variant was incorporated into simple spin-cast OLEDs with the following device structure: ITO / PEDOT:PSS (30 nm) / F8BT:Cl-Cl$_n$BsubNc (99:1 wt%) (30 nm) / TPBi (30 nm) / Ca (10 nm) / Ag (100 nm). This architecture was chosen based on our previous report of solution-processed silicon phthalocyanine-based host:guest OLEDs.[26] Metrics reported here are representative of 32 devices made from each derivative. Trends reported here were found to be consistent across these batches. Specific metrics presented here are for the highest performing device from each batch. Current-voltage-luminance data for the Cl-Cl$_n$BsubNc-based OLEDs is presented in Figure 3 alongside estimates for their frontier orbital energy levels. Corresponding performance metrics and typical spectral output characteristics are compiled in Table 2. Maximum EQEs above 1% are measured for the commercial Cl-Cl$_n$BsubNc OLEDs, with the remaining device types showing maximum EQEs between 0.82% and 0.96%. Maximum current efficiencies vary between 3.3 cd A^{-1} for the commercial Cl-Cl$_n$BsubNc OLEDs and 2.4 cd A^{-1} for the nitrobenzene Cl-Cl$_n$BsubNc OLEDs, with current efficiencies at brightness levels that are typical for display applications (100 cd m^{-2}) reaching a maximum of 2.5 cd A^{-1}. Peak electroluminescence red-shifts with the same trend as the peak photoluminescence.

Device studies suggest that with increased chlorination, there is a trade-off in achieving redder emission with a higher degree of chlorination at the cost of reducing PLQE. The trend in EQE is in keeping with the trend in PL lifetimes and PLQE in conjunction with the reduced FRET overlap from the host material in the redder analogues.

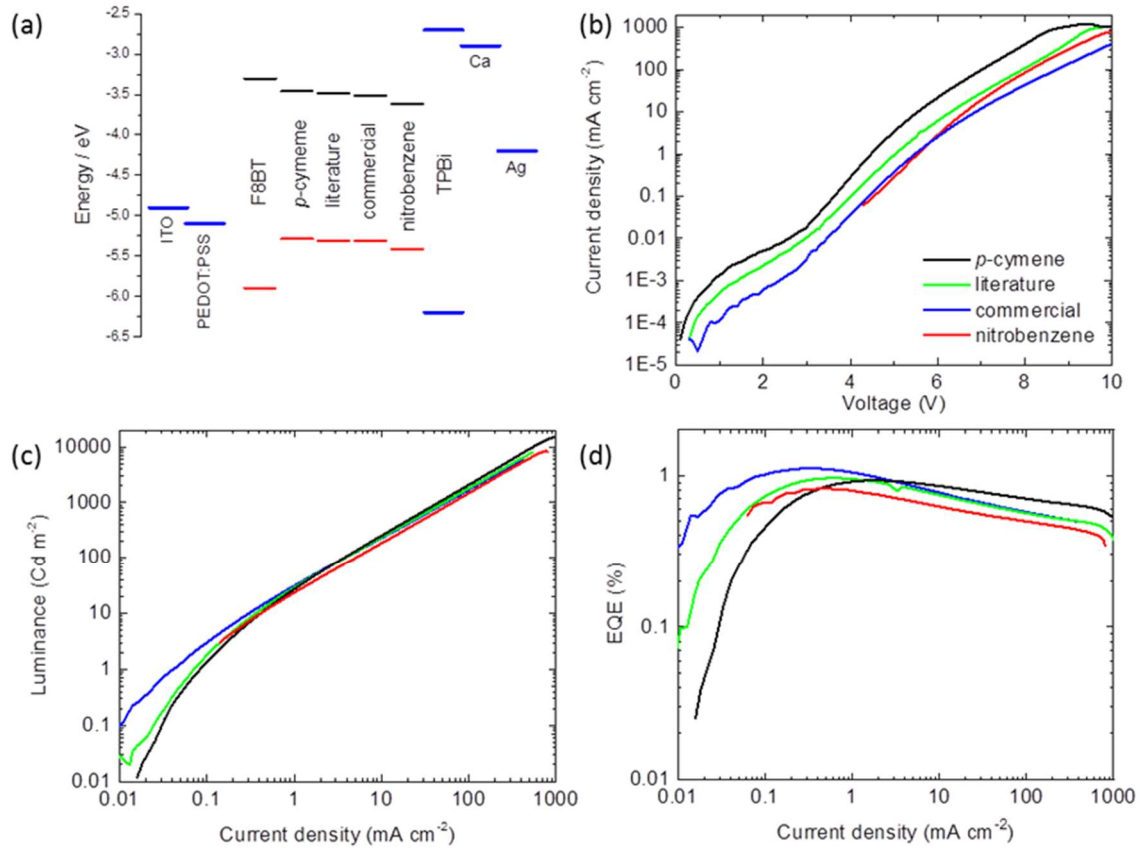

Figure 3. (a) Energy level diagram for the Cl-Cl$_n$BsubNc -based host-guest OLEDs. Current density-voltage characteristics are plotted in (b), with luminance and external quantum efficiency (EQE) data for the same devices plotted in (c) and (d) respectively. Data corresponding to the nitrobenzene device is truncated below 4.2 V due to electrical noise.

Table 2. Summary of OLED device characteristics. V_{ON} values correspond to a luminance of 1 cd m^{-2}. EL spectra measured at a device current density of 30 to 70 mA cm^{-2}.

	V_{ON} / V	EQE_{Max} / %	$J_{EQE,Max}$ / mA cm^{-2}	Current $efficiency_{Max}$ / cd A^{-1}	Peak EL / nm	Peak EL_{FWHM} / nm
***p*-cymene -Cl-Cl$_n$BsubNc**	3.7	0.93	1.73	2.75	677	33
literature -Cl-Cl$_n$BsubNc	3.3	0.96	0.61	2.85	683	36
Commercial -Cl-Cl$_n$BsubNc	4	1.12	0.30	3.31	685	37
nitrobenzene -Cl-Cl$_n$BsubNc	3.5 - 4	0.82	0.45	2.42	690	41

Insight into the spectral stability of the Cl-Cl$_n$BsubNc-based OLEDs was provided by current density-dependent EL measurements. Representative EL spectra are shown in Figure 4(a), with the guest contribution to the total EL as a function of OLED driving current density shown in in Figure 4(b). From Figure 4(a) it can be seen that EL from these OLEDs is overwhelmingly from the Cl-Cl$_n$BsubNc guest. By comparison with dilute solution and solid-state photoluminescence spectra, we conclude that guest electroluminescence arises primarily from isolated (i.e. non-aggregated) Cl-Cl$_n$BsubNc molecules. The wavelengths for peak EL are at most 3 nm red-shifted from the peak PL in dilute solution (Tables 1, 2 and S1) which suggests a negligible degree of aggregation. EL FWHM values are comparable to other BsubNCs in host:guest OLED architectures.[31–34] Data in Figure 4(b) shows a reversible decrease in the guest emission contribution to the overall EL with increasing current density. This general effect has been reported elsewhere, and attributed to more favourable radiative recombination in the host. This could be

due to a shift in the exciton recombination zone away from a guest-rich environment,[27,33,38] saturated guest emission and/or inefficient host:guest energy transfer. [28,33] Given the low guest concentration used in these OLEDs (1 wt%) and the relatively low PLQE of the nitrobenzene route Cl-Cl$_n$BsubNc (21%, see Table 2) we identify the latter processes as being more probable here.

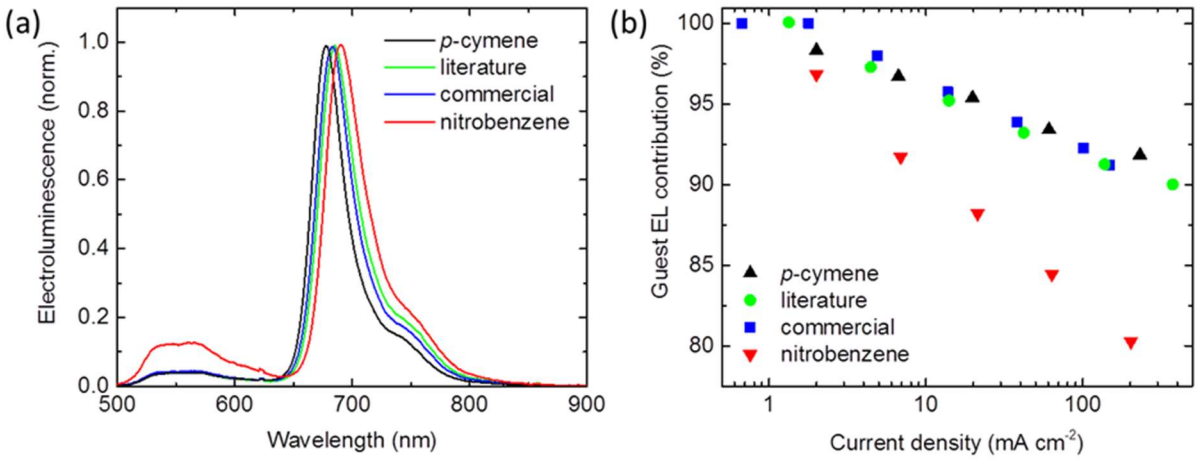

Figure 4. (a) EL spectra for each device, acquired at a current densities ranging between 30 and 70 mA cm^{-2}, normalized to the guest emission peak. In part (b) the relative contribution of Cl-Cl$_n$BsubNc emission to the overall OLED EL is presented. Values correspond to the ratio of integrated emission between 650 and 850 nm and overall emission between 500 and 850 nm.

Sources of host emission in F8BT have been shown to include TTA [39], however we attribute the dominant change in our system as most likely resulting from a reduction in FRET overlap. To determine whether the degree of bay position chlorination influences the photostability of the BsubNc within an OLED host matrix, representative films were subject to 30 minutes continuous photoexcitation (λ = 407 nm) in ambient conditions, with PL spectra recorded every 10 s. Data presented in Figure 4 and Figure S3 show that in all cases there was recovery of the host emission from the F8BT, indicating that the product of the photodegradation does not act as a deep trap site

for excitons. A similar effect was observed under voltage cycling, where higher current densities result in an irreversible drop in guest EL and an increase of host EL (Figures S5 and S6).

A range of degradation rates were observed between materials, but no clear correlation was found with the degree of bay chlorination. This may arise due to the range of Cl-Cl$_n$BsubNc variants present in each mixed alloyed sample. Establishing whether such a correlation exists, for instance through preferential formation of chloride radicals, would require isolation of differently halogenated species. Clearly the photo-bleaching kinetics are more complicated than a mono-exponential form. This could be attributed to a combination of different photo-stability of the differently chlorinated members of the ensemble, or the degraded molecular fragments acting as trap sites within the film.[40]

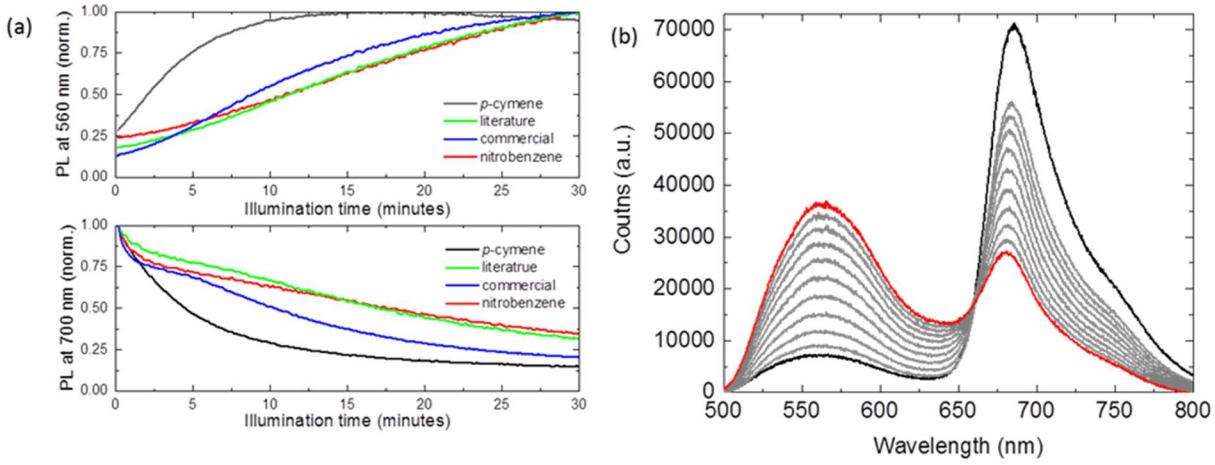

Figure 4. (a) Evolution in relative photoluminescence intensity from F8BT:Cl-Cl$_n$BsubNc host:guest films during continuous photoexcitation at 407 nm. The wavelengths 560 nm and 700 nm correspond to the peaks of the host and guest contributions respectively; intensities are normalized to the maximum values measured during the photoexcitation period. The general evolution in spectra is presented in (b) using data for F8BT:Cl-Cl$_n$BsubNc (nitrobenzene). Spectra

are shown from three minute intervals with the initial and final spectra highlighted black and red respectively.

Conclusions.

We demonstrate the degree of average bay-position chlorination in Cl-Cl$_n$BsubNcs influences a number of photophysical characteristics. In particular, a lower average degree of bay-position chlorination gives narrower, blue-shifted peak luminescence wavelength, increased luminescence quantum efficiency and decreased non-radiative decay rate. We show that solution processed OLEDs with EL dominated by narrow red emission from the dopant can be made using the mixed alloyed composition of Cl-Cl$_n$BsubNcs, with external quantum efficiency exceeding 1%. We find that lower average bay-position chlorination improved photoluminescence metrics, and the trend of device EQE at higher average chlorination was consistent with more rapid intersystem crossing reducing PLQE, combined with a reduction in FRET overlap with the host. This contrasts with the trend reported previously for OPV applications, whereby higher average bay-position chlorination was beneficial to device performance. These results suggest that no single Cl-Cl$_n$BsubNc design is superior for all optoelectronics applications. Instead, establishing synthetic routes towards pure materials of different chlorination fractions will likely allow tailored performance for device-specific optoelectronic applications. These materials demonstrate considerably narrower FWHM than both current TADF and phosphorescent materials, [41–43] supporting that progress into NIR OLEDs will likely require NIR hyperfluorescent dopants such as BsubNcs to help retain narrow emission rather than pure TADF systems.

Experimental.

Materials and solvents

F8BT (M_w 151k) was supplied by Cambridge Display Technology. Chlorobenzene and TPBi were purchased from Sigma Aldrich (#'s 284513 and 806781 respectively). All were used as-received without further purification. Evaporation grade Ca and Ag were purchased from Testbourne Ltd. and used as received.

Sample preparation

F8BT and Cl-Cl_nBsubNc were dissolved in chlorobenzene at concentrations of 20 mg mL^{-1} and 0.2 mg mL^{-1} respectively. Before use these stock solutions were stirred and heated at 70˚C for at least 48 hours and cooled to room temperature. Cl-Cl_nBsubNc solutions for photoluminescence measurements were further diluted in chlorobenzene to the desired concentration. F8BT:Cl-Cl_nBsubNc blend thin films of thickness 30 nm were prepared by spin coating blend solutions at 2000 rpm.

OLED fabrication

Devices were prepared by first cleaning ITO-coated glass substrates (15 Ω sq^{-1}, Colorado Concept Coatings) in warm acetone and 2-propanol in an ultrasonic bath. A 30 nm layer of PEDOT:PSS (Heraeus Clevios™ AI4083, pre-filtered using a 0.45 μm PVDF filter) was deposited via spin-coating at 5000 rpm and annealed at 130°C for 10 minutes under ambient conditions. After deposition of the active layer under glovebox conditions, a 30 nm layer of TPBi was deposited via spin-coating a 2 mg ml^{-1} MeOH solution at 2000 rpm. Samples were subsequently baked for 10 minutes at 60˚C before transfer to a vacuum chamber, where a bilayer back electrode of Ca / Ag

(10 nm / 100 nm) was deposited via thermal evaporation through an 8-pixel mask (typical deposition rates and vacuum pressures were 0.1 nm s^{-1} and 5 x 10^{-6} mbar respectively). The overlap between device anode and cathode defined an active area of 0.045 cm^2.

Optical spectroscopy characterisation

Measurements of Cl-Cl_nBsubNc optical density were made using a HP 8453 UV-VIS spectrometer in ambient conditions. Solutions were measured using quartz cuvettes (Hellma Analytics) with 1 mm path lengths. Photoluminescence measurements were made using an Edinburgh Instruments FLS980 Spectrometer with fixed excitation intensity and detection geometry. Quantum yield values were determined using an integrating sphere and a direct excitation method in a 10mm path length quartz cuvette. For PL lifetime measurements the time-correlated single photon counting (TCSPC) technique was used. Samples were excited with a 407 nm pulsed laser at 20 MHz repetition rate. Scattered light from the laser excitation was removed using an absorptive long-pass filter with a 430 nm edge. The photoluminescence was detected by a single-photon avalanche photodiode (SPAD) based on Si (MPD-PDM-PDF) with an instrument response of ca. 200 ps.

Solution-processed OLED Characterisation

Current - voltage characteristics were measured using a Keithley 2400 source measure unit. The light flux was measured simultaneously using a calibrated silicon photodiode located over the light-emitting pixel. Luminance in cd m^{-2} was calculated based on the emission spectrum of the LED, weighted against the standard luminosity function and the known spectral response of the silicon photodiode. The external quantum efficiency was calculated assuming a Lambertian emission profile. Electroluminescence spectra were measured using a Labsphere CDS-610 spectrometer.

Acknowledgements.

The authors acknowledge support from the EPSRC through the grant EP/M024873/1. This work was also supported by a Natural Sciences and Engineering Research Council (NSERC) Discovery Grant to TPB. D.C and S.T.E.J acknowledge the Royal Society for funding (grant numbers UF130278 and RG140472). The data underlying this publication are available at [url to be added in proof].

References.

[1] K. Cnops, B.P. Rand, D. Cheyns, B. Verreet, M.A. Empl, P. Heremans, 8.4% efficient fullerene-free organic solar cells exploiting long-range exciton energy transfer, Nat. Commun. 5 (2014) 3406. doi:10.1038/ncomms4406.

[2] J.D. Dang, D.S. Josey, A.J. Lough, Y. Li, A. Sifate, Z.-H. Lu, T.P. Bender, The mixed alloyed chemical composition of chloro-(chloro) $_n$ -boron subnaphthalocyanines dictates their physical properties and performance in organic photovoltaic devices, J. Mater. Chem. A. 4 (2016) 9566–9577. doi:10.1039/C6TA02457B.

[3] C. Duan, D. Guzmán, F.J.M. Colberts, R.A.J. Janssen, T. Torres, Subnaphthalocyanines as Electron Acceptors in Polymer Solar Cells: Improving Device Performance by Modifying Peripheral and Axial Substituents., Chemistry. 24 (2018) 6339–6343. doi:10.1002/chem.201800596.

[4] R.K. Garner, M.T. Dang, J.D. Dang, T.P. Bender, The Mixed Alloyed Chemical Composition of Chloro-(chloro) $_n$ -Boron Subnaphthalocyanines Dictates Their Performance as Electron-Donating and Hole-Transporting Materials in Organic Photovoltaics, ACS Appl. Energy Mater. 1 (2018) 1029–1036. doi:10.1021/acsaem.7b00180.

[5] Y. Bernhard, P. Richard, R.A. Decréau, Addressing subphthalocyanines and subnaphthalocyanines features relevant to fluorescence imaging, Tetrahedron. 74 (2018) 1047–1052. doi:10.1016/J.TET.2018.01.029.

[6] Y. Takao, T. Masuoka, K. Yamamoto, T. Mizutani, F. Matsumoto, K. Moriwaki, K. Hida, T. Iwai, T. Ito, T. Mizuno, T. Ohno, Synthesis and properties of novel fluorinated subnaphthalocyanines for organic photovoltaic cells, Tetrahedron Lett. 55 (2014) 4564–4567. doi:10.1016/J.TETLET.2014.06.069.

[7] K. Yamamoto, A. Takagi, M. Hada, R. Taniwaki, T. Mizutani, Y. Kimura, Y. Takao, K. Moriwaki, F. Matsumoto, T. Ito, T. Iwai, K. Hida, T. Mizuno, T. Ohno, Synthesis and optoelectronic properties of hexachloro- and hexaiodosubnaphthalocyanines as organic electronic materials, Tetrahedron. 72 (2016) 4918–4924. doi:10.1016/J.TET.2016.06.064.

[8] A. Takagi, T. Mizutani, Control of the molecular packing of chloroboron(iii) and fluoroboron(iii) subnaphthalocyanines by designing peripheral substituents, RSC Adv. 7 (2017) 54235–54245. doi:10.1039/C7RA11104E.

[9] J.D. Dang, D.S. Josey, M.T. Dang, T.P. Bender, Phenoxy-(Chloro)$_n$-Boron Subnaphthalocyanines: Alloyed Mixture, Electron-Accepting Functionality, and Enhanced Solubility for Bulk Heterojunction Organic Photovoltaics, ACS Omega. 3 (2018) 2093–2103. doi:10.1021/acsomega.7b01892.

[10] G.E. Morse, T.P. Bender, Boron Subphthalocyanines as Organic Electronic Materials, ACS Appl. Mater. Interfaces. 4 (2012) 5055–5068. doi:10.1021/am3015197.

[11] G. de la Torre, C.G. Claessens, T. Torres, Phthalocyanines: old dyes, new materials. Putting color in nanotechnology, Chem. Commun. 0 (2007) 2000–2015. doi:10.1039/B614234F.

[12] L. Bormann, F. Nehm, N. Weiß, V.C. Nikolis, F. Selzer, A. Eychmüller, L. Müller-Meskamp, K. Vandewal, K. Leo, Degradation of Sexithiophene Cascade Organic Solar Cells, Adv. Energy Mater. 6 (2016) 1502432. doi:10.1002/aenm.201502432.

[13] C.G. Claessens, D. González-Rodríguez, M.S. Rodríguez-Morgade, A. Medina, T. Torres, Subphthalocyanines, Subporphyrazines, and Subporphyrins: Singular Nonplanar Aromatic Systems, Chem. Rev. 114 (2014) 2192–2277. doi:10.1021/cr400088w.

[14] G. Löbbert, Phthalocyanines, in: Ullmann's Encycl. Ind. Chem., Wiley-VCH Verlag GmbH & Co. KGaA, Weinheim, Germany, 2000. doi:10.1002/14356007.a20_213.

[15] O.A. Melville, B.H. Lessard, T.P. Bender, Phthalocyanine-Based Organic Thin-Film Transistors: A Review of Recent Advances, ACS Appl. Mater. Interfaces. 7 (2015) 13105–13118. doi:10.1021/acsami.5b01718.

[16] N. Beaumont, S.W. Cho, P. Sullivan, D. Newby, K.E. Smith, T.S. Jones, Boron Subphthalocyanine Chloride as an Electron Acceptor for High-Voltage Fullerene-Free Organic Photovoltaics, Adv. Funct. Mater. 22 (2012) 561–566. doi:10.1002/adfm.201101782.

[17] K. L. Mutolo, E. I. Mayo, B. P. Rand, S. R. Forrest, M. E. Thompson*, Enhanced Open-Circuit Voltage in Subphthalocyanine/C_{60} Organic Photovoltaic Cells, J. Am. Chem. Soc. 2006, 128, 25, 8108–8109. doi:10.1021/JA061655O.

[18] P. Sullivan, A. Duraud, Ian Hancox, N. Beaumont, G. Mirri, J.H.R. Tucker, R.A. Hatton, M. Shipman, T.S. Jones, Halogenated Boron Subphthalocyanines as Light Harvesting Electron Acceptors in Organic Photovoltaics, Adv. Energy Mater. 1 (2011) 352–355. doi:10.1002/aenm.201100036.

[19] N. Beaumont, J.S. Castrucci, P. Sullivan, G.E. Morse, A.S. Paton, Z.-H. Lu, T.P. Bender,

T.S. Jones, Acceptor Properties of Boron Subphthalocyanines in Fullerene Free Photovoltaics, J. Phys. Chem. C. 118 (2014) 14813–14823. doi:10.1021/jp503578g.

[20] B. Ebenhoch, N.B.A. Prasetya, V.M. Rotello, G. Cooke, I.D.W. Samuel, Solution-processed boron subphthalocyanine derivatives as acceptors for organic bulk-heterojunction solar cells, J. Mater. Chem. A. 3 (2015) 7345–7352. doi:10.1039/C5TA00715A.

[21] G.E. Morse, J.L. Gantz, K.X. Steirer, N.R. Armstrong, T.P. Bender, Pentafluorophenoxy Boron Subphthalocyanine (F_5BsubPc) as a Multifunctional Material for Organic Photovoltaics, ACS Appl. Mater. Interfaces. 6 (2014) 1515–1524. doi:10.1021/am404179z.

[22] J.S. Castrucci, D.S. Josey, E. Thibau, Z.-H. Lu, T.P. Bender, Boron Subphthalocyanines as Triplet Harvesting Materials within Organic Photovoltaics, J. Phys. Chem. Lett. 6 (2015) 3121–3125. doi:10.1021/acs.jpclett.5b01254.

[23] C.D. Zyskowski, V.O. Kennedy, Compounds in the series from boron subphthalocyanine to boron subnaphthalocyanine, J. Porphyrins Phthalocyanines. 04 (2000) 649–654. doi:10.1002/1099-1409(200011)4:7<649::AID-JPP233>3.0.CO;2-4.

[24] N. Kobayashi, T. Ishizaki, and K. Ishii, H. Konami, Synthesis, Spectroscopy, and Molecular Orbital Calculations of Subazaporphyrins, Subphthalocyanines, Subnaphthalocyanines, and Compounds Derived Therefrom by Ring Expansion, J. Am. Chem. Soc. 1999, 121, 39, 9096–9110. doi:10.1021/JA983325C.

[25] V.Y. Artyukhov, A. V. Morev, Y.P. Morozova, V.A. Pomogaev, Investigation of the Heavy-Atom Effect on the Spectral-Luminescent Properties of Dichloroanilines, Russ. Phys. J. 45 (2002) 1203–1207. doi:10.1023/A:1023874504931.

[26] A.J. Pearson, T. Plint, S.T.E. Jones, B.H. Lessard, D. Credgington, T.P. Bender, N.C. Greenham, Silicon phthalocyanines as dopant red emitters for efficient solution processed OLEDs, J. Mater. Chem. C. 5 (2017). doi:10.1039/c7tc03946h.

[27] W. Hua, X. Du, W. Su, W. Lin, D. Zhang, Full phosphorescent white-light organic light-emitting diodes with improved color stability and efficiency by fine tuning primary emission contributions, AIP Adv. 4 (2014) 027103. doi:10.1063/1.4865209.

[28] F.-C. Chen, S.-C. Chang, G. He, S. Pyo, Y. Yang, M. Kurotaki, J. Kido, Energy transfer and triplet exciton confinement in polymeric electrophosphorescent devices, J. Polym. Sci. Part B Polym. Phys. 41 (2003) 2681–2690. doi:10.1002/polb.10648.

[29] K.L. Sampson, G.E. Morse, T.P. Bender, Does the Electron-Donating Polymer Design

Criteria Hold True for the Non-Fullerene Bulk Heterojunction Electron Acceptor Boron Subphthalocyanine? Yes, ACS Appl. Energy Mater. 1 (2018) 2490–2501. doi:10.1021/acsaem.8b00183.

[30] C. Duan, G. Zango, M. García Iglesias, F.J.M. Colberts, M.M. Wienk, M.V. Martínez-Díaz, R.A.J. Janssen, T. Torres, The Role of the Axial Substituent in Subphthalocyanine Acceptors for Bulk-Heterojunction Solar Cells, Angew. Chemie Int. Ed. 56 (2017) 148–152. doi:10.1002/anie.201608644.

[31] D.D. Díaz, H.J. Bolink, L. Cappelli, C.G. Claessens, E. Coronado, T. Torres, Subphthalocyanines as narrow band red-light emitting materials, Tetrahedron Lett. 48 (2007) 4657–4660. doi:10.1016/J.TETLET.2007.05.036.

[32] G.E. Morse, M.G. Helander, J.F. Maka, Z.-H. Lu, T.P. Bender, Fluorinated Phenoxy Boron Subphthalocyanines in Organic Light-Emitting Diodes, ACS Appl. Mater. Interfaces. 2 (2010) 1934–1944. doi:10.1021/am1002603.

[33] M.G. Helander, G.E. Morse, J. Qiu, J.S. Castrucci, T.P. Bender, Z.-H. Lu, Pentafluorophenoxy Boron Subphthalocyanine As a Fluorescent Dopant Emitter in Organic Light Emitting Diodes, ACS Appl. Mater. Interfaces. 2 (2010) 3147–3152. doi:10.1021/am100632y.

[34] T.G. Plint, B.H. Lessard, T.P. Bender, Doping chloro boron subnaphthalocyanines and chloro boron subphthalocyanine in simple OLED architectures yields warm white incandescent-like emissions, Opt. Mater. (Amst). 75 (2018) 710–718. doi:10.1016/J.OPTMAT.2017.11.028.

[35] M. Mac, A. Danel, K. Kizior, P. Nowak, A. Karocki, B. Tokarczyk, Investigations of the heavy atom effect occurring in bianthryl and 10,10′-dibromobianthryl. Fluorescence, cyclovoltamperometric and actinometric studies. Dedicated to Professor Dr Z. R. Grabowski and Professor Dr J. Wirz on the occasions of their 75th and 60th birthdays., Phys. Chem. Chem. Phys. 5 (2003) 988–997. doi:10.1039/b205842a.

[36] E.A. Gastilovich, V.G. Klimenko, S.A. Serov, R.N. Nurmukhametov, Nonradiative S-T intersystem crossing in α and β chlorine derivatives of naphthalene, Opt. Spectrosc. 106 (2009) 799–807. doi:10.1134/S0030400X09060046.

[37] J.C. Koziar, D.O. Cowan, Photochemical heavy-atom effects, Acc. Chem. Res. 11 (1978) 334–341. doi:10.1021/ar50129a003.

[38] J.-H. Hsu, H.-C. Su, Host-only solid-state near-infrared light-emitting electrochemical cells based on interferometric spectral tailoring, Phys. Chem. Chem. Phys. 18 (2016) 5034–5039. doi:10.1039/C5CP07065A.

[39] A. Dey, D. Kabra, Role of Bimolecular Exciton Kinetics in Controlling the Efficiency of Organic Light-Emitting Diodes, ACS Appl. Mater. Interfaces. 10 (2018) 38287–38293. doi:10.1021/acsami.8b10559.

[40] L. Song, E.J. Hennink, I.T. Young, H.J. Tanke, Photobleaching kinetics of fluorescein in quantitative fluorescence microscopy, Biophys. J. 68 (1995) 2588–2600. doi:10.1016/S0006-3495(95)80442-X.

[41] D.-H. Kim, A. D'Aléo, X.-K. Chen, A.D.S. Sandanayaka, D. Yao, L. Zhao, T. Komino, E. Zaborova, G. Canard, Y. Tsuchiya, E. Choi, J.W. Wu, F. Fages, J.-L. Brédas, J.-C. Ribierre, C. Adachi, High-efficiency electroluminescence and amplified spontaneous emission from a thermally activated delayed fluorescent near-infrared emitter, Nat. Photonics. 12 (2018) 98–104. doi:10.1038/s41566-017-0087-y.

[42] H. Ye, D.H. Kim, X. Chen, A.S.D. Sandanayaka, J.U. Kim, E. Zaborova, G. Canard, Y. Tsuchiya, E.Y. Choi, J.W. Wu, F. Fages, J.-L. Bredas, A. D'Aléo, J.-C. Ribierre, C. Adachi, Near-Infrared Electroluminescence and Low Threshold Amplified Spontaneous Emission above 800 nm from a Thermally Activated Delayed Fluorescent Emitter, Chem. Mater. 30 (2018) 6702–6710. doi:10.1021/acs.chemmater.8b02247.

[43] A. D'Aléo, M.H. Sazzad, D.H. Kim, E.Y. Choi, J.W. Wu, G. Canard, F. Fages, J.-C. Ribierre, C. Adachi, Boron difluoride hemicurcuminoid as an efficient far red to near-infrared emitter: toward OLEDs and laser dyes, Chem. Commun. 53 (2017) 7003–7006. doi:10.1039/C7CC01786C.

TOC Graphic

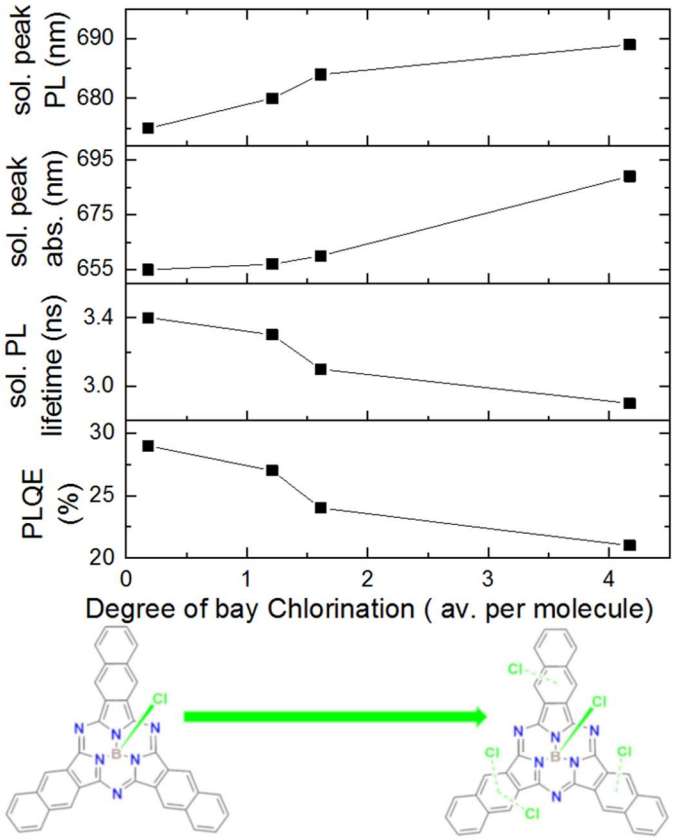
sol. peak PL (nm)
690
680
sol. peak abs. (nm)
695
675
655
sol. PL lifetime (ns)
3.4
3.0
PLQE (%)
30
25
20
0
1
2
3
4
Degree of bay Chlorination (av. per molecule)
Cl
N
B

Electronic supporting information.

Exploring the effects of bay position chlorination on the emissive properties of chloro-(chloro)$_n$-boron subnaphthalocyanines for light emission.

Saul T. E. Jones [a], *Andrew J. Pearson* [a], *Jeremy D. Dang* [b], *Neil C. Greenham* [a], *Timothy P. Bender* [*,b,c,d], *and Dan Credgington* [*,a]

[a.] Cavendish Laboratory, J.J. Thomson Avenue, Cambridge CB3 0HE, United Kingdom.

[b.] Department of Chemical Engineering and Applied Chemistry, University of Toronto, 200 College St., Toronto, Ontario, Canada M5S 3E5.

[c.] Department of Chemistry, University of Toronto, 80 St. George St., Toronto, Ontario M5S 3H6, Canada.

[d.] Department of Materials Science and Engineering, University of Toronto, 184 College St., Toronto, Ontario, Canada M5S 3E4.

Corresponding Authors

* - to whom correspondences should be addressed. Email: tim.bender@utoronto, dan.credgington@gmail.com.

Sections:

Chemical structures of differing degrees of bay chlorination

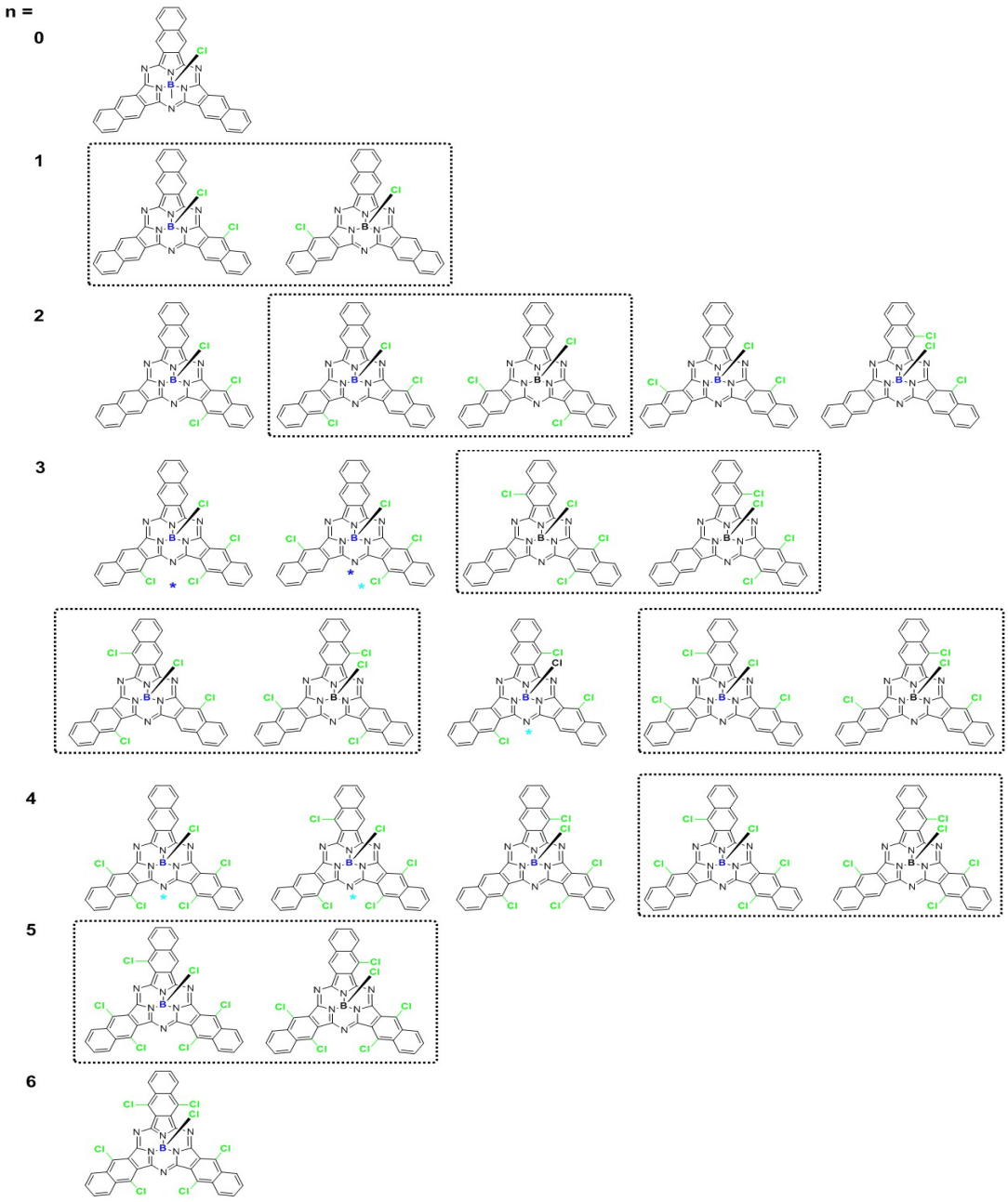

Fig. S1: Diagram of all possible bay-position chlorination configurations for Cl-Cl$_n$BsubNc where **n** denotes the number of additional chlorine atoms. In the main text ***n*** is used to describe the average degree of chlorination of each synthetic route.

1. Spectroscopy data

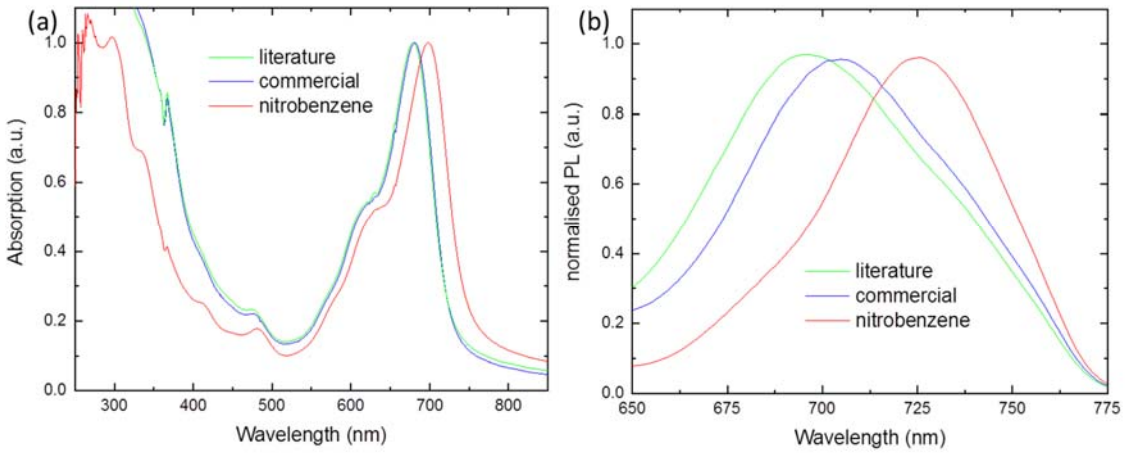

Fig. S2: Steady state absorption (a) and photoluminescence (PL) (b) spectra for solid films of Cl-Cl$_n$BsubNc prepared by thermal evaporation.

Table S1: Characteristic photophysical properties of the 4 mixed-bay position ensembles of Cl-Cl$_n$BsubNcs in different environments.

	Solution lifetime (ns)	Host:Guest lifetime (ns)	Peak solution PL (nm)	Peak Host:Guest PL (nm)	Peak Evap. PL (nm)	Solution peak abs. (nm)	Evap. film peak abs. (nm)	PL FWHM (nm)	PL FWHM (eV)
***p*-cymene -Cl-Cl$_n$BsubNc**	3.4	3.8	670	669	-	670	-	52	0.140
literature -Cl-Cl$_n$BsubNc	3.3	3.3	676	676	695	676	679	56	0.148
commercial -Cl-Cl$_n$BsubNc	2.9	3.3	684	685	724	684	681	58	0.152
nitrobenzene -Cl-Cl$_n$BsubNc	3.1	3.3	680	680	703	680	698	54	0.140

Table S1 confirms that Cl-Cl$_n$BsubNc photoluminescence from the Cl-Cl$_n$BsubNc:F8BT thin films is representative of Cl-Cl$_n$BsubNc in dilute population, as the peak photoluminescence wavelength and photoluminescence lifetimes are comparable to the dilute solution rather than the evaporated solid film.

2. Stability data

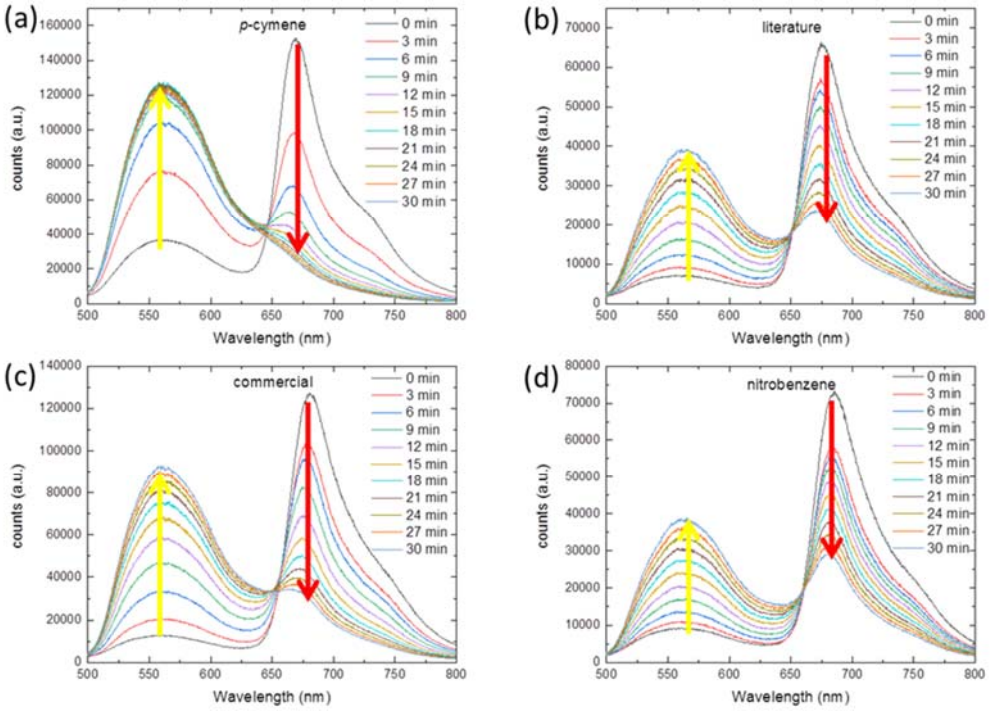

Fig. S3: Evolution in photoluminescence from Cl-Cl$_n$BsubNc:F8BT thin films subject to continuous photoexcitation (λ = 407 nm) over 30 minutes. Arrows indicate the direction of change with increasing time. No clear correlation between the observed kinetics and the average degree of Cl-Cl$_n$BsubNc bay-position chlorination was observed.

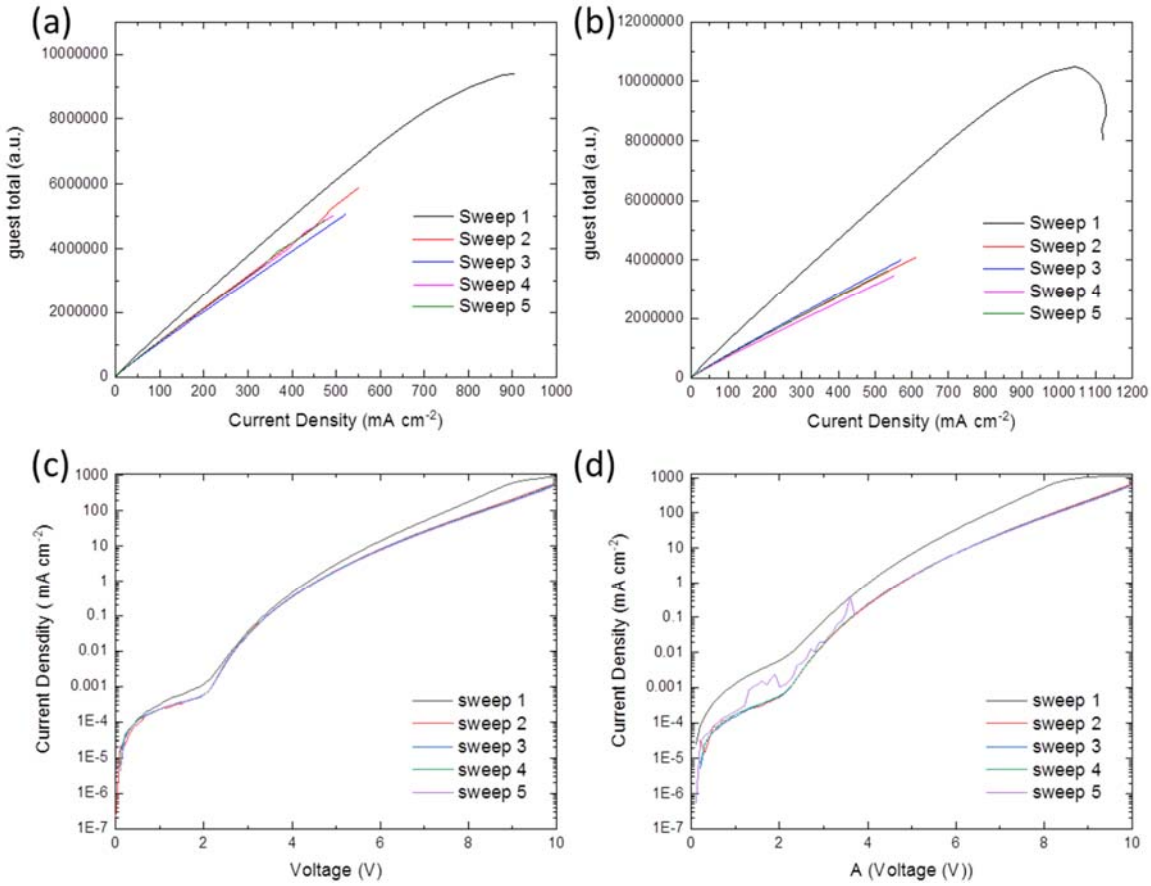

Fig. S4: Guest electroluminescence intensity as a function of current density (parts (a) and b)) and current density vs. voltage (parts (c) and (d)) for a literature (parts (a) and (c)) and a nitrobenzene (parts (b) and (d)) Cl-Cl$_n$BsubNc:F8BT OLED run through 5 consecutive cycles of 0 – 10V. For both device types a roll-off in electroluminescence intensity is observed at high current densities (sweep 1 data). The electroluminescence intensity is lower during subsequent cycles and is seemingly reversible. From these measurements we infer a drop in guest external quantum efficiency between sweep 1 and sweep 2.

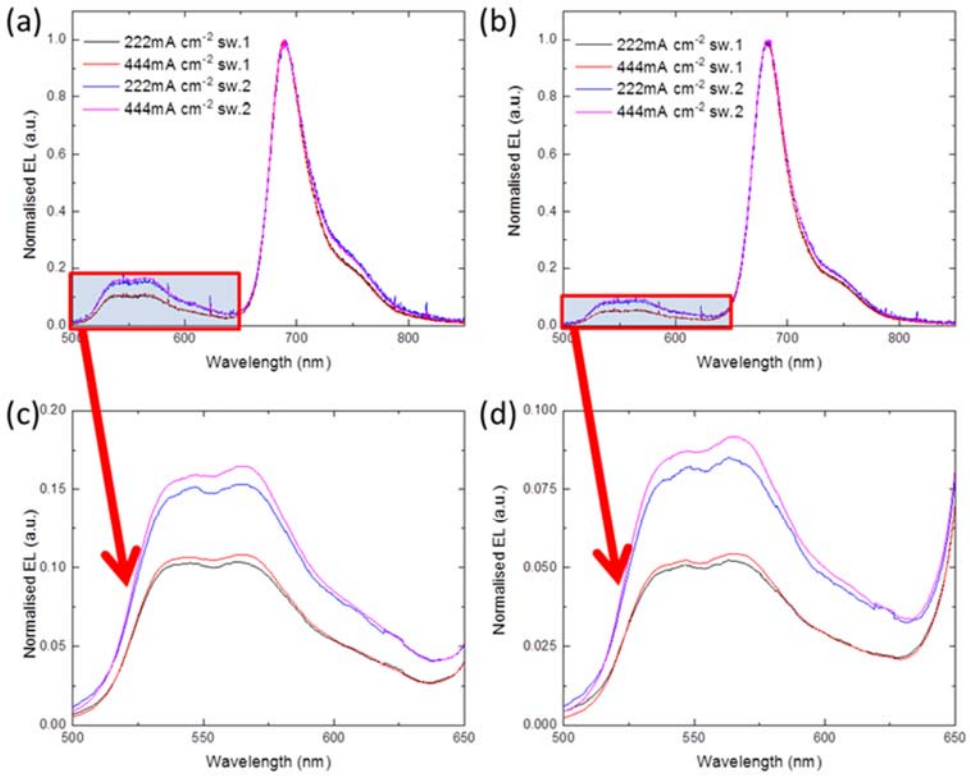

Fig. S5: Changes in F8BT contribution to the total OLED electroluminescence due to (1) high driving current densities (sweep 1 data) and (2) device degradation (sweep 2 data). Spectra from a nitrobenzene Cl-Cl$_n$BsubNc OLED are shown in parts (a) and (c) and spectra from a literature Cl-Cl$_n$BsubNc OLED are shown in parts (b) and (d).